Journal of Power Sources 182 (2008) 603–608

Contents lists available at ScienceDirect

Journal of Power Sources

journal homepage: www.elsevier.com/locate/jpowsour

Comparison of microchannel dimensions for air-breathing polymer exchange membrane microfuel cells

C.S. Spiegel [a,*], R. Agarwal [b], S. Bhansali [a]

[a] Department of Electrical Engineering, University of South Florida, Tampa, FL 33755, United States
[b] IMEC, Kapeldreef 75, B-3001 Leuven, Belgium

ARTICLE INFO

Article history:
Received 7 February 2008
Received in revised form 3 April 2008
Accepted 4 April 2008
Available online 18 April 2008

Keywords:
DRIE
Microchannels
PEM fuel cell
Flow field pattern

ABSTRACT

This paper evaluates proton exchange membrane (PEM) fuel cell microchannel width and depths ranging from 20 μm to 1000 μm. A DRIE process is employed to create the serpentine microflow field patterns from silicon wafers for channel width and depths ranging from 20 μm to 200 μm. To compare the smaller microchannel dimensions with conventional dimensions, computer numerical control (CNC) machining was used to create the 500 μm and 1000 μm flow field channel dimensions in delrin. All of the plates were coated with gold to prevent corrosion and to improve conductivity.

Two air-breathing 2.54 cm × 2.54 cm × 1.47 cm fuel cell stacks were designed and assembled for this research. The same membrane electrode assembly (MEA) with an active area of 1 cm^2 was tested with all of the silicon flow field plates with microchannels. The fuel cell performed well with the 20-μm width and depth flow channels (maximum power density of 65 W cm^{-2} or a maximum of 170 mA cm^{-2} at 0.2 V), although all of the *I–V* tests yielded good results for room temperature, air-breathing fuel cells. Microchannels with widths and depths from 100 μm to 20 μm look promising for new high-current density microelectro mechanical (MEMS) fuel cell designs.

1. Introduction

Fuel cells are set to become the power source of the future. In order to successfully design new fuel cells, an understanding of how all of the design and manufacturing processes influence performance variables is critical. Some of the design variables include flow channel geometry, catalyst particle size and shape, and electrolyte thickness. Understanding fuel cell microstructure is very important for optimizing fuel cell electrical behavior [1].

One of the most important fuel cell components is the flow field plates. These flow field plates are responsible for uniform fuel dispersion, efficient water removal, electric conductivity and mechanical sturdiness for the fuel cell membrane electrode assembly (MEA). Flow field plates in conventional fuel cells are typically made from stainless-steel or graphite, and traditional processes for creating the flow field pattern in flow field plates include computer numerical control (CNC) machining, injection molding and stamping. These materials and processes are not suitable for microelectro mechanical-based (MEMS) fuel cell systems. Typical materials that have been used for MEMS fuel cells in the literature are silicon wafers, carbon paper, polydimethylsiloxane (PDMS), SU-8 (EPON SU-8 epoxy resin from Shell Chemical), copper and stainless-steel metal foils. There have also been several studies that have investigated the creation of microchannels using MEMS techniques in the literature. Lee et al. [2] created flow channels in a silicon wafer with depths between 50 μm and 200 μm. The microfuel cell produced a current density of 50 mA cm^{-2}, which is typical performance for a microfuel cell. However, the efficiency could have been greatly improved if a non-corrosive metallic layer was applied to the silicon flow field plate to increase the conductivity. Yu et al. [3] had developed a reactive-ion etching (RIE) process on silicon wafers with a 200-μm flow channel depth. A conductive metal (0.5–1.5 μm Au, Cu or Ti) was sputtered on the surface of the silicon wafer. The results indicated that micro-featured flow field of the silicon-based flow field plates would provide more uniform distribution of fuels under the same operating conditions of gas pressure and flow rate over graphite flow field plates. Schmitz et al. [4] applied printed circuit board (PCB) processes for the manufacturing of flow field plates. The low current density obtained in this study may have been due to the shallow (35 μm) copper flow channel and poor conductivity of glass fiber substrate. O'Hayre et al. [5] designed a 16-cell proton exchange membrane (PEM) fuel cell in a 3.5-$in.^2$ glass fiber composite plate which had an open circuit voltage of 12 V for a 3C battery. However, there was still a large contact resistance, and the glass

* Corresponding author. Tel.: +1 7272301981; fax: +1 7272309035.
E-mail address: colleenspiegel@yahoo.com (C.S. Spiegel).

0378-7753/$ – see front matter © 2008 Elsevier B.V. All rights reserved.
doi:10.1016/j.jpowsour.2008.04.023

fiber substrate did not have enough mechanical strength to sustain the required stacking pressure.

Fuel cell performance should improve as the channel feature size decreases and gas flow velocity increases since the increased flow velocity enhances mass transport. However, a drawback of the smaller feature size is the increased pressure drop in the flow channels. The feature sizes for flow channels in the literature range from 100 μm × 200 μm × 20 μm to 500 μm × 500 μm to 750 mm × 750 mm × 12.75 mm, with many length, widths and depths in between with various rib widths [6–15]. However, there have been no studies conducted that compares the entire range of channel width and depth dimensions. In addition, there seems to be conflicting viewpoints regarding the performance of microchannels in the 20–500 μm range. For example, in Ref. [6] it mentions that better performance is gained between feature sizes of 483–99 μm, but the pressure losses under 200 μm are so large that it negates the effect of down-scaling [6]. In Ref. [7], when the channel depth was decreased from 1 mm to 300 μm, the power density performance increased by 71.9%. When the flow field channel depth was further reduced to 100 μm, the performance decreased by 8.6% [7].

In this paper, six different 1 cm^2 flow field patterns were created with various serpentine channel sizes ranging from 1000 μm to 20 μm in width and depth. The channels were designed to examine and compare the performance for different channel widths and depths in order to help to optimize microfuel cell dimensions. Two stacks were designed specifically for the flow field plates with the microchannels. Polarization curves were taken and analyzed for each flow field plate with different size microchannels with the same MEA and stack.

Table 1
Prototype stack dimensions

Stack dimensions	in.	mm
End plate	0.250	6.350
Gasket	0.004	0.102
Silicon flow channel plate	0.016	0.400
Gasket	0.004	0.102
MEA (fuel cell)	0.040	1.016
Silicon flow channel plate	0.016	0.400
End plate	0.250	6.350
Total thickness	0.58	14.72

2. Design and production of the microfuel cell stack and the silicon flow field plates with microchannels

Two fuel cell stacks were designed for this research. Fig. 1 schematically illustrates the fuel cell design. Each stack was 25.4 mm × 25.4 mm × 14.7 mm, and the dimensions of the fuel cell components are shown in Table 1. One stack used polyvinyl chloride (PVC) end plates, and the other used delrin end plates. These mate-

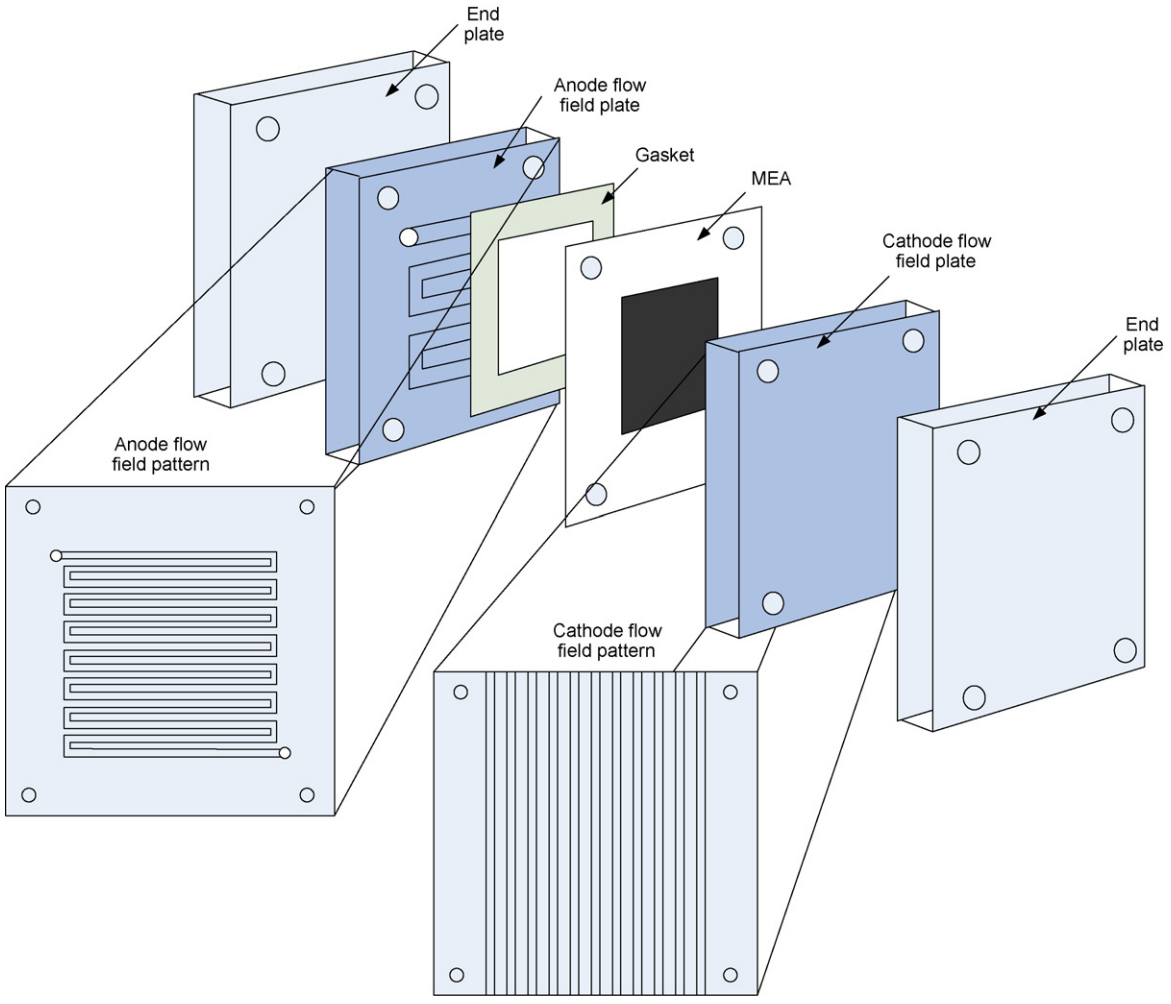

Fig. 1. Single cell design and its components.

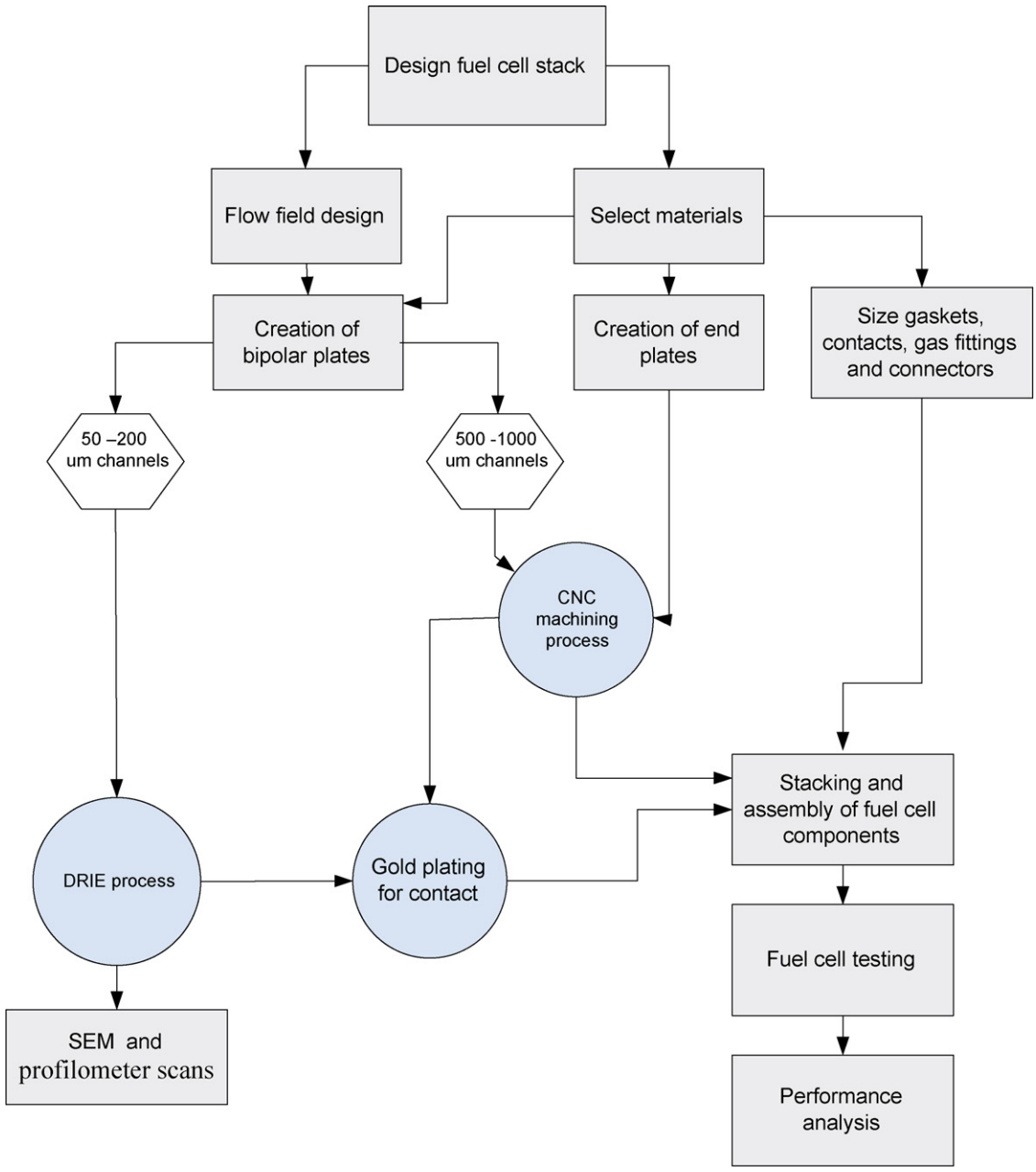

Fig. 2. Flow chart of research methodology.

rials were chosen because they are low-cost, and commercially available. Thin silicon gaskets were used to prevent gas leakage, and a contact layer was created by depositing a gold layer on the sides of the end plates that were in contact with the flow field plates.

The flow field plates were made from 400-μm thick, 4 in. silicon wafers. Two flow field plates for a single cell assembly were designed from a silicon wafer, with a total cell area of 6.45 cm^2 and a reaction area of 1 cm^2. A deep reactive-ion etching (DRIE) fabrication process was used for the fabrication of microflow fields in the silicon wafer for the 200–20 μm depth. In order to compare the silicon DRIE fabricated flow field plates with conventional machining and dimensions, four additional plates made of delrin were made using traditional CNC machining processes with flow field channel dimensions of 500 μm and 1000 μm. As shown in Table 2,

Table 2
Flow field plate channel dimensions

No.	Channel width (μm)	Channel depth (μm)	Rib (Gap) width (μm)	% of active area that is channels	No. of channels and ribs	Channel length
1	1000	1000	1000	50.0	4	7
2	500	500	500	50.0	8	7.5
3	200	200	200	50.0	20	7.8
4	100	100	100	50.0	40	7.9
5	50	50	50	50.0	80	8.0
6	20	20	20	50.0	200	8.0

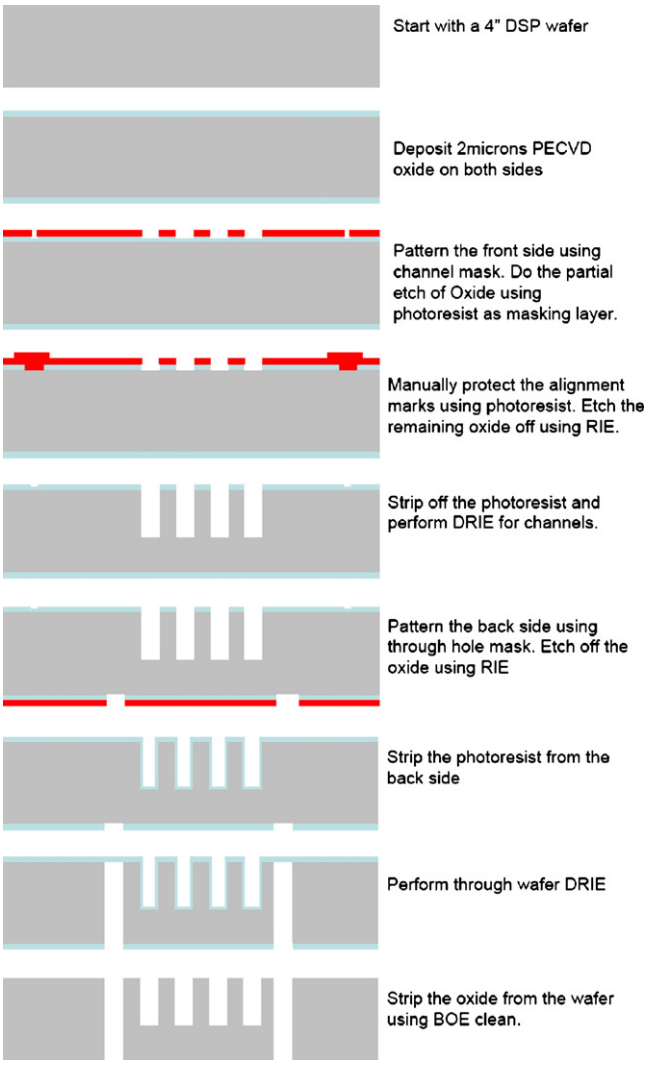

Fig. 3. Flow chart of the RIE process used for the creation of the flow field plates.

the width and depth of the flow channels ranged from 1000 μm to 20 μm, with a consistent channel area of 50% (channel to rib ratio of 1:1). The channel length range was from 7.8 mm to 8.0 mm, and the width of the ribs also ranged from 1000 μm to 20 μm.

The serpentine flow field design was chosen because it has been shown to perform the best in several MEMS fuel cell studies [6,7]. The serpentine flow path is continuous from start to finish. An advantage of the serpentine flow path is that it reaches the entire active area of the electrode by eliminating areas of stagnant flow.

In order to promote conductivity and reduce contact resistance, all of the flow field plates were coated with gold. The openings in the inlet and outlet of the gas channel plates were made substantially larger than the flow field channel dimensions in order to fit easy-to-find connectors for gas flow into the stack.

The thinness and fragility of the flow field plates required careful handling during stacking and assembly. Two single cell stacks were assembled for cell performance tests. The flow chart of research methodology is presented in Fig. 2.

2.1. Microchannel fabrication process

A 2-μm thick PECVD SiO_2 layer was deposited on both sides of the Si wafer. The front side was patterned using the channel mask and Futurex PR2000 photoresist. RIE was then performed for 10 min

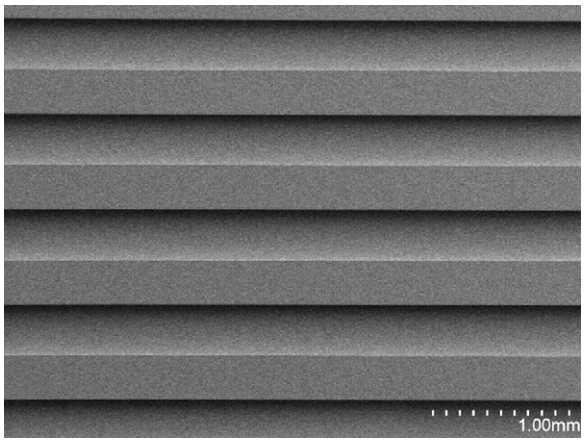

Fig. 4. Microflow field channels in silicon flow field plate.

to partially etch the exposed SiO_2. Next, Shipley 1813 photoresist was manually placed over the alignment marks, and then baked for 1 min at 90 °C. RIE is performed again for 60 min to etch off the remaining SiO_2. The photoresist was then stripped off using acetone/methanol. The wafer was then put into DRIE, and etched ($\sim$1 μm min^{-1}) to the desired depth of the channels.

Along with the microchannels, through holes were made in the same silicon wafer in order for the silicon flow field plate to be placed into the fuel cell stack. PR2000 was spun onto the back side of the wafer, and then RIE of SiO_2 was performed for 70 min. Through wafer DRIE was then performed to create the through holes. The last step for creating the through holes was stripping off the oxide layer using BOE. A layer of Ti/Au 300 nm/1 μm was then sputtered on the wafer from the channel side (front side) to prevent corrosion and improve conductivity. The processes used to create the flow field pattern are presented in Fig. 3, and further details of the fabrication process can be found in Ref. [16].

3. Results and discussions

3.1. The two stage DRIE process

In order to create the microflow fields and through holes in the silicon flow field plates, two iterations of the etching process are conducted. The first iteration of etching process is to create the main flow field channel pattern. The second iteration of etching process is to create the through holes for the gas inlet, outlet and

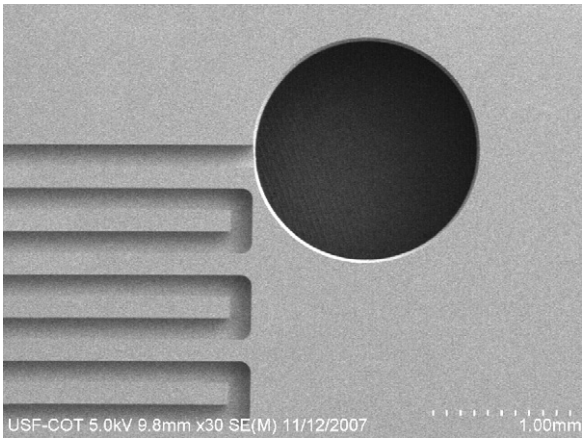

Fig. 5. Through hole added to microflow field channels in silicon flow field plate.

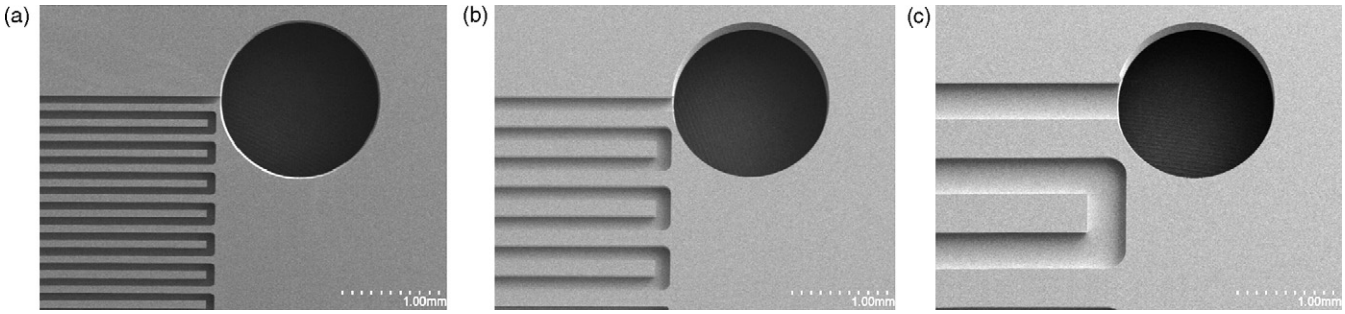

Fig. 6. SEM images of microflow field channels and through holes: (a) 20 μm, (b) 50 μm, and (c) 200 μm width channels.

through bolts. Fig. 4 shows the main flow channels. Fig. 5 shows the through hole with the microflow channels.

The scanning electron microscopy (SEM) and profiler scans were employed to exam the surface profile and depth of the flow channel. Fig. 6 compares the microflow field channels at 20 μm, 50 μm and 200 μm. The SEM photos demonstrate the precision of the microchannel structure created by the DRIE process.

3.2. Single cell fuel cell stack performance tests

Two single cell, air-breathing fuel cell stacks were assembled for fuel cell performance tests. A five-layered MEA from Clean Fuel Cell Energy is used, which is composed of Nafion 112, GDL of carbon cloth material and 1 mg cm^{-2} of Pt loading on both the anode and cathode. The active fuel cell area is 1 cm × 1 cm. The same MEA and stack is used with the different microflow field plates (20–200 μm flow channels). A second stack was assembled for the 500 μm and 1000 μm channel flow field plates. The single cell fuel cell stacks are shown in Fig. 7.

Five cell performance tests are conducted with 0.5 standard cubic centimeter per minute (SCCM) of hydrogen from an electrolyzer, with no additional humidification. All tests are taken at 25 °C and an ambient pressure. *I–V* curves of these cell performance tests are plotted in Figs. 8 and 9. The 1000 μm and 500 μm flow channels had the worst cell performance characterized by low current densities, high contact resistance and poor mass transfer.

The fuel cell stack was designed as a scaled-down version of a conventional fuel cell to enable comparison with both larger commercial fuel cells, and with other MEMS fuel cells in the literature. The designs presented in this paper were used to understand the effect of channel and rib dimensions to optimize the design of a MEMS fuel cell. Some of the benefits of the MEMS flow regime include laminar flow, higher velocities, rapid diffusion, low leakage, surface effects, good flow control and very small dead volumes. A major advantage in designing MEMS fuel cells are that many of the layers can be applied through sputtering (or some other process), which means that they can be extremely thin, which will make the future stacks lighter and less costly with high current densities. Some of the issues that maybe encountered when designing MEMS fuel cells are surface roughness, uneven topography, bubbles and flooding in flow channels.

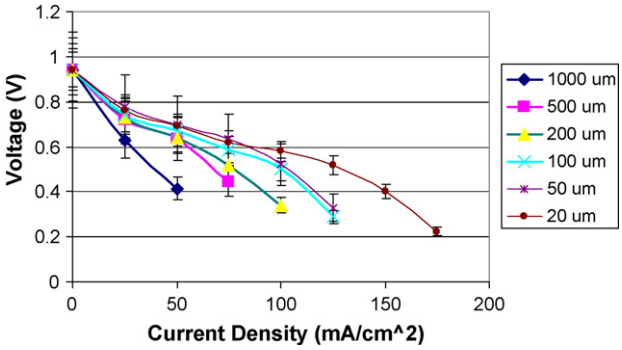

Fig. 8. *I–V* curve of the cell performance tests.

The flow field channels (20–1000 μm) increase in performance with the decrease in channel width, depth and rib size (space between flow channels). The 20 μm flow channel width, depth and rib size outperformed all other channel sizes in terms of power density and current density. In the activation polarization dominated region (~0.8–1.0 V), all of the activation voltage losses were about the same for all of the fuel cell tests conducted. This was expected since the same fuel cell MEA was used, therefore, the activation voltage losses due to the electrode kinetics should be similar.

Fig. 7. Prototypes of the single cell fuel cell stacks.

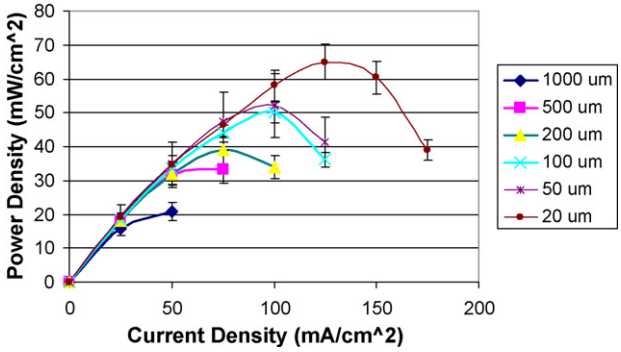

Fig. 9. Fuel cell power density curves for 20–1000 μm channel widths and depths.

In the ohmic polarization dominated region (~0.5–0.8 V), the 20 μm flow channel width, depth and rib size clearly performed better in terms of voltage and current density. Since the majority of the ohmic resistance in fuel cells is the electrolyte, and the same MEA was used, the difference in ohmic resistance is due to the difference in channel width, depth, rib size, the number of channels and the percent channel area. As shown in Table 2, the percent area of channel and rib space (50%) is consistent for all of the flow field plates. The decreased contact resistance for the flow field plates with the 20 μm dimensions may be due to the gas diffusion media protruding into the flow channel. This provides greater surface area of the GDL layer in contact with the flow field plates.

The concentration polarization dominated region (~0–0.5 V) displays the largest difference between polarization curves for the dimensions of the flow field plates. As the channel width and depth decreases from 1000 μm to 20 μm, the velocity and pressure drop increase rapidly. The large increase in pressure drop is counteracted by the rapid increase in velocity. Although the channel to rib ratio is identical for all of the flow field plates created (1:1), the decrease in rib size may aid in better overall reactant flow through the gas diffusion media since the "void space" between channels is decreased. In addition, since the depth of the 20 μm is substantially less than the other depths, the stagnant flow region at the interface between the channel and gas diffusion media encompasses a larger portion of the flow channel. Also, if the gas diffusion media is protruding into the channels, this stagnant flow region may encompass a large portion of the channel, and therefore, the flow in the channel enters the diffusive regime with greater ease than in larger channels where the flow has to convert from convective to diffusive.

Although the performance of the MEMS fuels presented in this paper performed better than most other MEMS fuel cells in the literature, the performance is still poor in comparison to convectional fuel cells where the current density typically reaches 1–1.5 A cm^{-2} (0.5–8.0 A cm^{-2} for free-convection fuel cells). One of the issues with MEMS fuel cells is that liquid water droplets generated at the cathode can block a flow channel entirely. These blockages can lead to reactant starvation at the cathode, which not only affects the concentration polarization region of the polarization curve, but also affects the fuel cell performance through reaction kinetics (the activation polarization region) due to the dependence upon the reactant and product concentrations at the reaction sites. In addition, when the reactants are deficient at the reactant sites, this generates less charge, therefore, the amount of charge that is transported through the cell is reduced, which contributes to the ohmic polarization dominated region. The combination of these voltage losses creates a total polarization curve with poor performance in comparison to traditional fuel cells.

4. Conclusions

Two air-breathing MEMS fuel cell stacks were designed and built using the methodology of a scaled-down version of a conventional fuel cell stack. The fuel cell active area was 1 cm^2, with a total area of 6.45 cm^2 (1 $in.^2$). Flow field plates with channel widths, depths and rib sizes of 1000–20 μm were created, tested and compared using the same MEA.

A DRIE process is employed to create the serpentine microflow field patterns from a silicon wafer for the fuel cell channel width and depths ranging from 20 μm to 200 μm. The fuel cells performed the best with the 20-μm width, depth and rib dimensions (maximum power density of 65 W cm^{-2} or a maximum of 170 mA cm^{-2} at 0.2 V), although all of the *I–V* tests yielded good results for room temperature, free-convection microfuel cells. The 20 μm dimensions allowed increased channel velocity, rapid diffusion and homogenous reactant distribution along the flow channel. Smaller flow channel dimensions (>100 μm) appear to be promising for future microfuel cell technologies.

References

[1] C.K. Dyer, J. Power Sources 106 (2002) 31–34.
[2] S.J. Lee, S.W. Cha, Y. Liu, R. O'Hayre, F.B. Prinz, Electrochemical Society Proceedings, Spring, 2000.
[3] J. Yu, P. Cheng, Z. Ma, B. Yi, J. Power Sources 124 (2003) 40–46.
[4] A. Schmitz, M. Tranitz, S. Wagner, R. Hahn, C. Hebling, J. Power Sources 118 (2003) 162–171.
[5] R. O'Hayre, D. Braithwaite, W. Hermannb, S.J. Lee, T. Fabian, S.W. Cha, Y. Saito, F.B. Prinz, J. Power Sources 124 (2003) 459–472.
[6] S.W. Cha, R. O'Hayre, Y. Saito, F.B. Prinz, J. Power Sources 134 (2004) 57–71.
[7] C.W. Wong, T.S. Zhao, Q. Ye, J.G. Liu, J. Power Sources 155 (2006) 291–296.
[8] J.G. Liu, T.S. Zhao, Z.X. Liang, R. Chen, J. Power Sources 153 (2006) 61–67.
[9] R.S. Hahn, Wagner, A. Schmitz, H. Reichl, J. Power Sources 131 (2004) 73–78.
[10] S.-S. Hsieh, C.F. Huang, J.K. Kuo, H.H. Tsai, S.H. Yang, J. Solid State Electrochem. 9 (2005) 121–131.
[11] Q. Lu, C.Y. Wang, J. Power Sources 144 (2005) 141–145.
[12] D. Modroukas, V. Modi, L.G. Frechette, J. Micromech. Microeng. 15 (2005) S193–S201.
[13] W. Li, C. Liang, W. Zhou, J. Qui, Z. Zhou, G. Sun, Q. Xin, J. Phys. Chem. B 107 (2003) 6292–6299.
[14] Q. Lu, C.Y. Wang, T.J. Yen, X. Zhang, Electrochim. Acta (2004) 821–828.
[15] S.-J. Lee, Y.-P. Chen, C.-H. Huang, J. Power Sources 145 (2005) 369–375.
[16] R. Agarwal, S. Samson, S. Kedia, S. Bhansali, J. Microelectromech. Syst. 16 (2007) 122–129.